Accepted Manuscript

Novel superparamagnetic micro-devices based on magnetised PLGA/PLA microparticles obtained by supercritical fluid emulsion and coating by carboxybetaine-functionalised chitosan allowing the tuneable release of therapeutics

Cricchio Vincenzo, Mark Best, Ernesto Reverchon, Nicola Maffulli, Gary Phillips, Matteo Santin, Della Porta Giovanna

PII: S0022-3549(17)30358-1

DOI: 10.1016/j.xphs.2017.05.005

Reference: XPHS 807

To appear in: *Journal of Pharmaceutical Sciences*

Received Date: 1 March 2017

Revised Date: 26 April 2017

Accepted Date: 2 May 2017

Please cite this article as: Vincenzo C, Best M, Reverchon E, Maffulli N, Phillips G, Santin M, Giovanna DP, Novel superparamagnetic micro-devices based on magnetised PLGA/PLA microparticles obtained by supercritical fluid emulsion and coating by carboxybetaine-functionalised chitosan allowing the tuneable release of therapeutics, *Journal of Pharmaceutical Sciences* (2017), doi: 10.1016/j.xphs.2017.05.005.

Novel superparamagnetic micro-devices based on magnetised PLGA/PLA microparticles obtained by supercritical fluid emulsion and coating by carboxybetaine-functionalised chitosan allowing the tuneable release of therapeutics

Cricchio Vincenzo[1], Mark Best[2], Ernesto Reverchon[1], Nicola Maffulli[3], Gary Phillips[2], Matteo Santin[2(**)], Della Porta Giovanna[1,3(*)]

[1] Supercritical Fluids Lab., Department of Industrial Engineering, University of Salerno, Via Giovanni Paolo II, 84084 Fisciano (SA), Italy.

[2] Brighton Studies in Tissue-mimicry and Aided Regeneration (BrightSTAR), Brighton Centre for Regenerative Medicine (BCRM), University of Brighton, Huxley Building Lewes Road, Brighton, UK.

[3] Translational Medicine Lab., Department of Medicine, Surgery and Dentistry, University of Salerno, Via S. Allende, 84081 Baronissi (SA), Italy

(*) Corresponding Author: Della Porta Giovanna, Laboratory of Translational Medicine - Department of Medicine, Surgery and Dentistry "Scuola Medica Salernitana", University of Salerno, Via S. Allende, Baronissi (SA) 84084, Italy. e-mail: gdellaporta@unisa.it; tel: +39089964104; fax: +39089964057. Room 002.

(**) co-Corresponding Author: Matteo Santin, Brighton Studies in Tissue-mimicry and Aided Regeneration (BrightSTAR), Brighton Centre for Regenerative Medicine (BCRM), University of Brighton, Huxley Building Lewes Road, Brighton, UK.

ABSTRACT

When superparamagnetic nanoparticles are loaded within micro-carriers of thermosensitive and injectable biopolymers, "*smart*" microdevices are obtained: they respond to an external magnetic field (EMF) through the release of any co-encapsulated molecules with a remote on-off control.

Creating reliable and effective fabrication technologies for the production of these *smart* nano/micro-devices remains a challenge. In this work Supercritical Emulsion Extraction technology (SEE) is proposed for the fabrication of microcapsules with a core of *poly-lactic-co-glycolic acid* (PLGA) or *poly-lactic acid (PLA)* covered by carboxybetaine-functionalized chitosan (*f-chi*) and loaded with paramagnetic nanoparticles (MAG, mean size of 6.5±3.0 nm) and water soluble fluorescein (Fluo). Fluo is co-encaspulated as a fluorescent marker for the release study.

Microcarriers showed a mean size of 800±60nm with an encapsulation efficiency of up to 90%. The inversion of surface charge, after the *f*-chitosan coating, suggested the presence of a uniform functionalized surface available for further chemical linkage. The external chitosan layer had a thickness of 200±50nm. An excellent MAG dispersion was confirmed within the biopolymer matrix that was shown to be responsive to EMF; indeed, Fluo was released over 3 or 5 days from PLGA or *f-chi*PLGA microdevices into PBS medium at 37°C; whereas, remote on-off controlled release was achieved when an Alternating Magnetic Field (AMF) was applied.

INTRODUCTION

Superparamagnetic nanoparticles embedded within biopolymer microcarriers may offer several therapeutic advantages in a number of clinical applications. The biopolymer coating can enhance their biocompatibility, prevent leaching and improve dispersability[1-2]; additionally, in the case of thermosensitive behavior of the biopolymer chosen for coating, a fixed dose of the co-encapsulated molecule can be released by remote control[3-4].

The possibility of treating cancer by induced hyperthermia has led to the development of many different devices designed to heat malignant cells while sparing surrounding healthy tissue[5-6]. The frequency and strength of the externally applied magnetic field is obviously limited by deleterious physiological responses to high frequency magnetic fields[7-8]. However, hyperthermia can be an effective local adjuvant therapy for carcinomas and sarcomas; as an example, a randomized phase III trial showed that regional hyperthermia combined with neo-adjuvant chemotherapy for soft tissue sarcomas resulted in better local progression-free survival than chemotherapy alone[9]. Several reports suggested that hyperthermia for osteosarcoma achieved an effective response, including the induction of apoptosis[10] and inhibition of tumor proliferation[11] and DNA synthesis[12] *in vitro*. Regional hyperthermia using an alternating magnetic field reduced the pulmonary metastasis of osteosarcoma in an *in vivo* study[13]. Recent studies indicated that hyperthermia contributes to the improvement of the prognosis of patients with soft tissue sarcomas; however, few reports have evaluated the impact of hyperthermia on tumor cell motility, which is an important factor of metastasis[14].

The use of a targetable magnetic device is an appealing treatment option as it can offer a better way of ensuring that the intended target tissue is heated and/or a localised drug delivery is obtained by an on-demand actuation mechanism. The second option is obtained using thermosensitive polymers[15] or silica[16], which can serve as coating materials for magnetic nanoparticles and trigger the release of a drug in an on-off mode in response to a

magnetically induced increase of temperature. A large variety of magnetic microdevices have been proposed in the literature to deliver drugs to specific target sites. Generally, the magnetic component of the particle is coated with a biocompatible polymer to shield the magnetic particle from the surrounding environment[17-19] and/or can also be functionalized by attaching carboxyl or amine groups[20]. Magneto liposomes[21] and porous metallic nanocapsules[22] have also been described.

In vivo studies utilising magnetic carriers loaded with doxorubicin have already been applied to sarcoma tumors implanted in rat tails[23] and the initial results were encouraging, showing a total remission of the sarcomas compared to no remission in another group of rats which were administered with ten times the drug dose but without magnetic targeting. In addition, success in cytotoxic drug delivery and tumor remission has been reported by several groups using animal models including rats[24] and swine[25]. More recently, an in vitro study reported that magnetic poly-lactide-co-glycolide nanocarriers co-encapsulated with doxorubicin were easily internalized into murine Lewis lung carcinoma cells inducing apoptosis[26]. Other authors have described magnetic microdevices with functional properties of magnetic resonance imaging[27] or as magnetic actuation for noninvasive remote-controlled drug release[28] or as on-demand release of multifunctional nanocapsules[29].

Due to its significant biodegradability and biocompatibility, PLGA/PLA has been approved in drug delivery systems for parenteral administration by the FDA and the European Medicine Agency. Moreover, the possibility of sustained release and targeted nano and microparticle delivery to specific organs or cells lends these materials to other clinical applications. As a consequence, *poly-lactide* (PLA) and its *glycolide co-polymer* (PLGA) have been utilized as a magnetide carrier and different fabrication technologies have been described including a single step coaxial electro-hydrodynamic atomization technique[30] (Gun

et al., 2013), conventional solvent evaporation methods[31-38], supercritical technology[39] and chemical synthesis[40-41].

An engineered size distribution, coupled with excellent nanoparticle and drug co-encapsulation efficiency, is a very important fabrication parameter for the industrial production of microcapsules, ensuring their controlled and reproducible manufacture. Reliable and effective fabrication technologies able to satisfy all these parameters and assure economically adequate encapsulation efficiency (higher than 80%) remain a challenge. In fulfilling this objective, supercritical fluid technologies have been described that offer improved control over the morphology and composition of micro and nanoparticles[42-44] (or biomaterial porosity)[45]. Among all the supercritical technologies described in the literature for micro and nanoparticle fabrication Supercritical Emulsion Extraction (SEE) was recently described as the most effective method for the fabrication of biopolymer microcapsules, due to the fact that it uses supercritical carbon dioxide for the fast extraction of the emulsion oily phase (oil-in-water or multiple water-oil-water) achieving the production of microcapsules with excellent encapsulation efficiency. This technology has recently been developed with a continuous process operation layout that assures a greater uniformity of product[46-47].

However, PLGA/PLA showed low potential to modify the surface properties to provide better interaction with biological materials. Recently, aqueous solutions of zwitterionic carboxybetaine derivatives have drawn special attention, due to their anti-fouling properties which have been shown to resist a wide variety of protein adsorption, biofilm formation and cell attachment[48]. Carboxybetaine also provides the capability of further biomaterial functionalisation[49]. The overall hydration property of carboxybetaine is ascribed to its ability to form hydrogen-bonded interactions with a range of organic and inorganic acids owing to a high electron density on its two carboxylic oxygen atoms.

The aim of this paper is to explore the performance of SEE in the fabrication of PLA and PLGA injectable microcapsules carrying superparamagnetic nanoparticles (MAG) loaded with fluorescein (Fluo), a typical fluorescent probe. The microdevices were coated with chitosan functionalised with carboxybetaine moieties to improve surface biocompatibility of the microsystem. Different emulsion compositions were processed by SEE to identify the best emulsion stability and formulation to obtain the highest encapsulation efficiency and an engineered drug release with or without the ability to control release remotely using an external magnetic field.

MATERIALS & METHODS

Materials

CO_2 (99.9%) was purchased from SON (Naples, Italy). Poly-Vinyl Alcohol (PVA, Mol wt: 30000–55000), poly-Sorbate (Tween 80), Fluorescein sodium salt (Fluo, water solubility 500 g/L), Iron Oxide nanoparticles (Fe_3O_2, mean size 6.5 nm ±3.0 nm; plus oleic acid, as stabilizer) were used in water suspension as received from Sigma-Aldrich Co., (Milan, Italy). Poly-lactic acid (PLA, RESOMER® RG 203H; Mol wt: 20.000) and Poly-lactic-co-glycolic acid (PLGA 50:50, RESOMER® RG 504H, Mol. wt: 38000-54000) were obtained from Evonik Industries (Essen, Germany). Ethyl acetate (EA, purity 99.9%), was supplied by Carlo Erba Reagents (Milan, Italy).

Emulsion preparation and Supercritical Emulsion Extraction apparatus

Different *water-oil-water* (w_1-o-w_2) emulsions (ratio 1:19:80 w/w) were prepared to load MAG and/or Fluo into the biopolymer capsules, respectively. The oil phase was always prepared by dissolving 2 g of PLA or PLGA in 19 g of ethyl acetate. The internal water phase (w_1) was of 1 mL of water/PVA solution (0.06 % w/w) with a fixed amount of MAG (2.5, 5,

10 mg) and/or Fluo (10 mg), respectively; the external water phase (w_2) was 80 g of EA-saturated water solution with Tween80 (0.6% w/w) in water. The primary emulsion (w_1-o) was obtained by sonication for 1 min at 30% of tip sonicator amplitude (mod. S-450D, Branson Ultrasonics Corporation, Danbury, CT, USA); the w_1-o emulsions were, then, immediately mixed into the external water phase by high-speed stirring (mod. L4RT, Silverson Machines Ltd., Waterside, CheshamBucks, UK) for 3 min at 3300 rpm. The emulsion stability was monitored by Optical Microscopy; stable emulsions were loaded into the column (height 1600 mm, internal diameter 10 mm) packed with stainless steel packings (Pro-Pak, 4 mm nominal size, 0.94 voidage) by high pressure piston pump (mod. 305, Gilson, France) at the top of the column and contacted to supercritical-CO_2 pumped by a second high pressure diaphragm pump (mod. Milroyal B, Milton Roy) from the bottom. Before starting the emulsion delivery, the column was wetted with a fixed amount of the water phase. A separator located downstream at the top of the column was used to recover the extracted solvent. The nanocarrier suspension was continuously collected at the bottom of the extraction column using a needle valve, and washed with pure water by centrifugation prior their lyophilization.

Droplet and microsphere morphology

Droplets in the emulsion were observed using an optical microscope (OM, mod. BX 50 Olympus, Tokyo, Japan) equipped with a phase contrast condenser. Microspheres shape and morphology were investigated by Field Emission-Scanning Electron Microscopy (FE-SEM, mod. LEO 1525, Carl Zeiss SMT AG, Oberkochen, Germany) coupled with energy dispersive X-ray spectroscopy (EDX, INCA Energy 350, UK) and by the same FE-SEM equipped with an S-TEM detector (mod. Zees Ultra Plus, Carl Zees SMT AG, Oberkochen, Germany). For FE-SEM observation samples of powder were placed on a double-sided adhesive carbon tape previously stuck to an aluminum stub and coated with a thin chromium

film (layer thickness 250 Å) using a sputter coater (mod.108 A, Agar Scientific, Stansted, United Kingdom).

Chitosan functionalisation and microspheres coating

Chitosan was dissolved in acetic acid and diluted 1:1 with methanol before *N*-succinylating with 4% (w/v) succinic anhydride in acetone solution (SC). This step was followed by the grafting of betaine monomers previously activated through reaction with 10X Molar excess N-(3-dimethylaminopropyl)-N-ethylcarbodiimide hydro-chloride (EDC) and 25X Molar excess N-hydroxysuccinimide (NHS) in 0.1M MES buffer pH 6.0. SC-B was desalted into dH_2O using dialysis with 3.5kDa MWCO cellulose tubing and syringe filtered at 0.45µm before lyophilising. The synthesis of both the derivatised chitosan and final *f*-Chi was assessed by FTIR. Functionalisation was assessed on chitosan samples in powdered form using the Perkin Elmer Spectrum 65 with a universal ATR sampling accessory. A total of 8 scans were obtained between 650 cm^{-1} and 4000 cm^{-1} (at 4 cm^{-1}) per sample.

To obtain *f*-chitosan-coated microdevices (*f*-ChiPLGA), the microcapsules, as recovered after the SEE process (at pH 3.9 due to the presence of CO_2, still dissolved in water), were centrifuged and re-suspended in 50M acetic acid buffer to reach a chitosan solution of 0.4 mg/mL and incubated for 1 h at room temperature. After incubation, the uncoated chitosan was removed by an ultra-centrifugation and washing step in phosphate buffer at pH 7, repeated twice.

Microcapsule size distributions and suspension Zeta-Potential

Particle size distributions (PSD) were measured using a Mastersizer S apparatus (mod. Mastersizer S, Malvern Instruments Ltd., Worcherstershire, United Kingdom), based on dynamic light scattering (DLS). Analyses were performed immediately after the preparation of the emulsions and of the microsphere suspensions, using several milligrams of each sample, appropriately diluted with distilled water.

A Zetasizer (mod. NanoZS Malvern Inc., Wocherstershire, UK) equipped with a 5.0 mW He-Ne laser operating at 633 nm was used for Zeta-Potential measurements. Samples were analyzed in glass cuvettes at 25°C and scattering angle of 173°; all the results are based on an average of 3 measurements, which was calculated on an average of 10 runs. Zeta-Potential value expressed in mV indicates the potential difference between the dispersion medium and the stationary layer of fluid attached on the dispersed particle and is a key indicator of the dispersion stability.

The electrical characteristics of free MAG and PLA/PLGA microcarriers were analyzed by electrophoresis measurements as a function of pH using the Malvern Zetasizer. In this assay, different solutions of NaCl (0.001M) in NaOH or HCl at pH values ranging from 3 to 11 were prepared using a pH meter (Mettler Toledo, France). Zeta potential of diluted suspensions was tested to determine the pH effect on the MAG loaded microapsules[50].

Solid state characterization

MAG encapsulation efficiency was measured by thermogravimetric analysis (TGA), as the residue remaining after total combustion of the polymeric component of the particles. 4 mg of each sample was placed in alumina crucibles and heated up to 600°C at a rate of 10 °C/min, under a constant air flow of 50 N cm^3/min. The infrared spectra were recorded with a Unicam Mattson 5000 FT-IR Spectrometer at room temperature. The spectra were taken in KBr discs in the range of 3500-400 cm^{-1}.

Drug loading and in vitro release study

Fluo was measured fluorimetrically (λex 460 nm; λem 515 nm) using a spectrofluorimeter (mod. Infinite™ 200 series, InsTecan Group Ltd., Männedorf, Switzerland). Encapsulation Efficiency of Fluo was measured by dispersing an accurately weighed amount (approximately 20 mg) of microcarriers in 1 mL of acetone and then diluted

with 20 mL of distilled water. Encapsulation Efficiency (EE%) percentage was expressed as Fluo amount detected/Fluo amount loaded x 100.

In vitro release data were obtained by suspending 20 mg of microcarriers in 3 mL of physiological solution at room temperature and stirred continuously. Every 24 h the samples were centrifuged at 2 g for 15 min and the supernatant was completely removed and replaced with fresh media to maintain sink conditions. Released Fluo concentrations from collected samples were then assayed fluorimetrically. Release experiments were performed in triplicate and curves are the mean profile obtained; error bars are also reported to better describe the data. Triggered release was monitored by weighting 20 mg of microdevices, dispersing them into 4 mL of physiological solution within a petri dish on top of the solenoid and subjected to an Alternating Magnetic Field (AMF) of strength 2.98 kA/m and frequency 297 kHz. The rise in surface temperature of nanocomposites was recorded by IR camera. The AMF was continued for 5 min and the released Fluo concentrations were assayed fluorimetrically. The experiment was repeated every hour and the Fluo released after the magnetic field exposure was then monitored by centrifuging at 2 g for 15 min, sampling the supernatant and replacing with fresh media.

RESULTS AND DISCUSSION

Microcarrier fabrication: operative SEE conditions,

Microcarriers were produced by processing different emulsion formulations by SEE at operative pressure and temperature conditions of 9 MPa and 38°C, respectively, with a countercurrent SC-CO_2 flow rate of 1.4 kg/h and an Liquid/Gas ratio of 0.1 on mass based[46]. The operative conditions used were selected in order to achieve a fast and complete extraction of ethyl acetate, the oily phase of the emulsion. Indeed, using these pressure and temperature conditions a complete miscibility between carbon dioxide and ethyl acetate is

obtained; whereas, no miscibility with the water external phase is possible. Moreover, under these conditions, carbon dioxide has a density of about 0.3 gcm^{-3} and a good density difference is assured between the gas and the liquid moving in a countercurrent fashion within the packed column; these operative conditions assured a fast, effective and complete ethyl acetate extraction after only 5 minutes of residence time in the apparatus. The SEE layout also allows the continuous recovery of the microdevices, so they have no chance of aggregating or re-organizing their structure. The operative pressure, temperature and flow rate ratio conditions described in this work are different from those described by *Furlan et al*.[39] where the authors reported the production of magnetic nanocomposites in a PLGA matrix via supercritical fluid extraction of emulsion. In addition, they used a different process layout that works in a semi-continuous arrangement that involves two streams mixed by spraying them with two nozzles at the inlet of the reactor. In this configuration, the particles remain suspended in the water phase throughout the whole process and they are recovered only after reactor depressurization, therefore some rearrangements and aggregation of the particles are possible.

Microcarrier sizes and loadings

Figure 1 shows the SEM micrographs of PLGA and PLA microcarriers; they are spherical, with mean sizes ranging between 800 and 900 nm and a standard deviation not higher than 10% of the mean value; their mean sizes did not show any influence with respect to different MAG loadings. Emission Differential X-ray-Scanning Electron Microscope (EDX-SEM) analyses suggested a good iron dispersion within the biopolymer matrix, as illustrated in **Figure 2,** where the red map in the micrograph indicates iron atomic X-ray emission (the data reported refers to PLGA/MAG loaded at 2.5 mg/g). Good encapsulation efficiency was also suggested from the iron percentage calculated by the X-ray emissions. In **Figure 3** TGA traces are reported to describe the thermal behavior of three different carrier

formulations from which was calculated the iron oxide amount after samples were heated to 750°C. Encapsulation Efficiency was 99% for all PLGA samples and 90% for PLA devices. Mean sizes (MSs) and standard deviation (SDs) of all the prepared devices with different MAG loading are listed in **Table 1**, together with the nominal MAG loading and the measured values.

The MAG loaded within the polymer matrix was also clearly detected by FT-IR. Indeed, as illustrated in **Figure 3,** the FT-IR spectra of the different formulations fabricated showed the characteristic absorption peak for Fe_3O_4 at 580 cm^{-1} in agreement with other works[51], and those of the poly-esters that are evident at about 1750 cm^{-1} (carbonyl groups), 1080 cm^{-1} (C–O–C stretching bands) and 1450 cm^{-1} (C–H stretching in methyl groups). The IR traces therefore confirmed a good dispersion and encapsulation of magnetite within the matrix of the PLGA and PLA devices fabricated by SEE. All the emulsion formulations tested here provided improved encapsulation efficiency when compared with those reported in the literature[31,39].

The excellent encapsulation efficiency obtainable by SEE processing is due to the short residence time of the emulsion/suspension in the high pressure packed column that caused fast polymer hardening. However, when the amount of magnetite loaded was more than 5 mg/g, evident nanoparticle agglomerates on the microcarrier surface were observed by SEM, suggesting ineffective entrapment; as a consequence, only microdevices with a MAG loading below 5 mg/g will be further discussed. This result seemed somewhat in contrast with those reported by *Liu et al.*[32] that described biopolymer microcarriers with a magnetite content of 40-60%; however, distorted surface morphology was always reported by the authors. In our case, to assure a triggered release, MAG loading between 0.5-1% were selected, also to avoid the stronger thermal side effect that higher MAG loading may have.

Carriers Surface stability

Surface charge is one of the most important parameters governing tissue uptake of particles. Zeta Potential is a useful indicator of surface charge, and it can be employed as an index reflecting the stability of the microdevices obtained. Moreover, it has been mentioned that the surface properties of magnetite are extremely sensitive to pH fluctuations. However, such properties should not be found when magnetite crystals are well encapsulated in the interior of PLA or PLGA nanoparticles. Thus, we investigated the influence of pH on the Zeta-potential in water suspension for all of the SEE produced microcarriers. Synthesized magnetite crystals show an obvious isoelectric point in the vicinity of pH 6.7 accompanied by a negative potential in alkaline pH medium and a positive one in acidic pH medium[50]. This data was confirmed and demonstrated in **Figure 4** (see black square dots). However, surface charges of the magnetic microcarriers (for all the formulas tested with PLA and PLGA) were not influenced by the pH values as also illustrated in **Figure 4,** where the zeta potential of particles was found to be less positive (negative) than that of magnetite at acid (basic) pH values. This leads to the confirmation that magnetite is very well encapsulated within the microdevices.

f-Chitosan coating

FTIR spectra of functionalized chitosan showed a reduction of the peaks attributed to the primary amine groups (peak 1564 cm^{-1}) of the chitosan following the chemical grafting of the betaine molecules. Further evidence to support the successful grafting of these carboxybetaine moieties on the material was provided by the increased methyl peak formation at 2937 cm^{-1} (consistent in the betaine only spectra), and in the aliphatic amine region of peaks between 1020 cm^{-1} and 1220 cm^{-1} (see also **Figure 3**)

f-Chi was used to coat MAG loaded PLA and PLGA microcarriers at concentrations of 0.4 mg/mL, and the resulting Zeta-potentials of these coated microspheres were also

compared to those of the uncoated samples. Indeed, the uncoated PLA and PLGA nanoparticles showed a negative Zeta Potential at pH 4.75 of -8.1± 1.2 mV; when they were covered with *f*-chitosan the Z-Potential value increased up to 26 ± 1.2 mV at pH of 5.5 for both samples (see red and blue rhombus in **Figure 4**). This inversion of Zeta potential towards positive values demonstrated the successful coating of the beads whereby *f*-Chi exposing carboxybetaine and remaining non-functionalised amino groups of chitosan contribute to the change of surface charge. In both cases, the adsorption of chitosan occurred spontaneously, with no aggregation of the colloids.

In **Figure 5** an FE-SEM image and a TEM image of PLGA carriers loaded with MAG at 5 mg/g and coated with *f*-chitosan are illustrated; the coating did not alter the spherical shape of the structure, but generated slightly irregular carrier surfaces. FE-SEM images of PLA coated microdevices loaded with MAG at 5 mg/g are also illustrated in **Figure 5**. The covered microcapsules also showed an increase in mean size from 921 nm to 1100 nm in the case of PLGA and from 839 nm to 1098 nm in the case of PLA microdevices, as represented by the histograms reported in **Figure 5,** where the PSDs of the coated and uncoated devices are compared, for both PLGA and PLA formulations. No increase in the size distribution was monitored. From the mean size increases the chitosan layer was calculated to range between 100-125 nm. The *f*-chitosan coating improved MAG encapsulation efficiency that was measured at 99% for both PLGA and PLA devices. It can be speculated that the chitosan coating (performed just after SEE processing) prevents a washing off for the MAG nanoparticles (9-10% of the loading) present on the microcarrier surface by facilitating their stronger adhesion to the microcarrier surface. The improved drug loading efficiency can also be ascribed to the ability of carboxybetaine to entrap solutes by their highly hydrated molecular structure via hydrogen bonding[52].

Sustained release

The cumulative amount of Fluo released (%) vs. time (days) from uncoated and *f*-chitosan coated PLGA microspheres is illustrated in **Figure 6**. Experimental points over the complete assay time are presented in the scatter plot with the standard deviation (three replicates were performed). Almost 60% of loaded Fluo was released in the first day; this "burst" effect is typical for small and highly water soluble molecules loaded in less than 1 micron devices. From day two, Fluo showed a sustained release, with an amount of 8% of the load released each day for the following 5 days. The *f*-Chi coating reduced to one half the Fluo "burst" release, and further delayed the overall release of the Fluo. Indeed, only 34% of the loaded molecule was released in the first day, followed by a slower release of 5.5%/day of the loaded amount. From the coated microdevice, two thirds of the Fluo load was released per day when compared to the uncoated devices and, therefore, the total release time was increased to 10 days. The reduction of the bust release and the slower overall Fluo release observed for the *f*-Chi coated devices can again be speculated to be further controlled by carboxybetaine and its ability to entrap solutes within their highly hydrated molecular structure.

Triggered release by Alternating Magnetic Field (AMF)

Magnetite nanoparticles with a size generally less than 30 nm exhibit super paramagnetism[53]. Thus, the encapsulated magnetite was expected to have superparamagnetic properties and the produced microspheres were exposed to an AMF to demonstrate remote control release. In detail, microdevices with different compositions, PLGA, *f-chi*PLGA and PLA all loaded with 8 mg/g of Fluo and 4 mg/g of MAG, were exposed to an AMF and the amount of Fluo released are plotted in **Figure 6,** against time; the AMF input is also shown. All microcarriers performed an on-off release of the loaded Fluo. MAG/PLGA microdevices showed a triggered release with 40%, 30% and 20% of the encapsulated Fluo released during

the first 3 spots; whereas, a lower amount of Fluo was released in each of the first three spots from the coated *f-chi*PLGA (36%, 28% and 10%, respectively) suggesting that the *f*-Chi coating reduced the dose emitted in each spot. The PLA nanocarrier released an amount between 25 and 18 % of the loaded Fluo in the first three spots, and then 10% of the loaded molecules for the subsequent three spots. The results indicated that a good remote control release was obtainable from the described microdevices and the possibility of engineering the amount delivered in each spot varied according to the microcarrier formulation.

CONCLUSIONS AND PERSPECTIVES

The advantage of the proposed approach is the combination of the emulsification method with the use of the supercritical fluid technology that offers a robust and fast way to fabricate engineered microcarriers, with excellent encapsulation efficiency and good magnetic nanoparticle dispersion within the biopolymer matrix. The approach also proposed an effective carboxybetaine-functionalized chitosan coating of the microcarriers that opens new routes of investigation for a controlled release of drugs combined with enhanced biocompatibility properties.

However, the behaviors of the microsystems proposed were described *in vitro* by using a simulated physiological medium with microspheres always well dispersed. As we move to an *in vivo* biological environment, specific surfactants and/or additives have to be considered for the injectable formulation in order to assure the good dispersion of the locally hosted microsystems and to prevent large particle aggregation that may eventually occur[54-55]. Therefore, further studies will involve an *in vivo* testing of the formulation proposed on animal models with a specific follow up that will also include the post-mortem microscopy as a primary technique for qualitatively assessing the state of dispersion of the microsystem proposed.

REFERENCES

[1] Pankhurst, Q.A., Connolly, J., Jones, S.K., Dobson, J., 2003. Applications of magnetic nanoparticles in biomedicine, J. Phys. D: Appl. Phys., 36, 167-181.

[2] Tartaj, P., Morales, M., Veintemillas-Verdaguer, S., Gonzalez-Carreno, T., Serna, C.J., 2003. The preparation of magnetic nanoparticles for applications in biomedicine, J. *Phys. D: Appl. Phys.*, 36, 182-197.

[3] Dobson, J., 2008. Remote control of cellular behaviour with magnetic nanoparticles, *Nature Nanotechnology*, 3, 139-143.

[4] Mura, S., Nicolas, J., Couvreur, P., 2013. Stimuli-Responsive Nanocarriers For Drug Delivery, *Nature Materials*,12, 991-1003.

[5] Van der Zee, J., 2002. Heating the patient: a promising approach? *Ann. Onco.*, 13, 1173-1184.

[6] Wust, P., Hildebrandt, B., Sreenivasa, G., Rau, B., Gellermann, J., Riess, H., Felix, R., Schlag, P.M., 2002. Hyperthermia in combined treatment of cancer, *Lancet Oncol*., 3, 487-97.

[7] Jordan, A., Scholz, R., Maier-Hau, K., Johannsen, M., Wust, P. Nadobny, J., Schirra H., Schmidt, H., Deger, S., Loening, S., Lanksch, W., Felix, R., 2001. Presentation of a new magnetic field therapy system for the treatment of human solid tumors with magnetic fluid hyperthermia, *Journal of Magnetism and Magnetic Materials*, 225, 118-126.

[8] Granov, A.M., Muratov, O.V. Frolov, V.F. 2002. Problems in the local hyperthermia of inductively heated embolized tissues, *Theor. Foundations Chem. Eng*., 36, 63-66.

[9] Issels, R.D., Lindner, L.H., Verweij, J., Wust, P., Reichardt, P., Schem, B.C., Rahman, S.A., Daugaard, S., Salat, C., Wendtner, C.M., Martin, C., Vujaskovic, Z.

Wessalowski, R., Jauch, K.W., Dürr, H.R., Ploner, F., Melnyk, A.B., Mansmann, U., Hiddemann, W., Blay, J.Y., Hohenbergere, P. 2010. Neo-adjuvant chemotherapy alone or with regional hyperthermia for localised high-risk soft-tissue sarcoma: a randomised phase 3 multicentre study, *Lancet Oncol*., 11, 561-570.

[10] Alcaide, M., Ramírez-Santillán, C., Feito, M.J., de la Concepción Matesanz, M., Ruiz-Hernández, E., Arcos, D., Vallet-Regí, M., Portolés, M.T. 2012. In vitro evaluation of glass-glass ceramic thermoseed-induced hyperthermia on human osteosarcoma cell line, *J Biomed Mater Res Part A* 100A, 64-71.

[11] Trieb, K, Blahovec, H, Kubista, B. 2007. Effects of hyperthermia on heat shock protein expression, alkaline phosphatase activity and proliferation in human osteosarcoma cells, *Cell Biochem Funct*., 25, 669-672.

[12] Shui, C., Scutt, A. 2001. Mild heat shock induces proliferation, alkaline phosphatase activity, and mineralization in human bone marrow stromal cells and Mg-63 cells in vitro. *J Bone Miner Res.*, 16, 731-741.

[13] Shido, Y., Nishida, Y., Suzuki, Y., Kobayashi, T., Ishiguro, N. 2010. Targeted hyperthermia using magnetite cationic liposomes and an alternating magnetic field in a mouse osteosarcoma model, *J Bone Joint Surg Br*., 92, 580-585.

[14] Nakajima, K., Yanagawa, T., Watanabe, H., Takagishi, K. 2012. Hyperthermia reduces migration of osteosarcoma by suppression of autocrine motility factor, *Oncol Rep*., 28(6), 1953-1958.

[15] Hua, M.Y. Liub, H.L., Yanga, H.W., Chenc, P.Y., Tsaie, R.Y., Huangc, C.Y., Tsengc, I.C., Lyub, L.A., Mab, C.C., Tangb, H.J., Yenf, T.C., Wei, K.C. 2011. The effectiveness of a magnetic nanoparticle-based delivery system for BCNU in the treatment of gliomas, *Biomaterials*, 32, 516-527.

[16] Zhang L, Wang T, Yang L, Liu C, Wang C, Liu H, Wang YA, Su Z 2012. General route to multifunctional uniform yolk/mesoporous silica shell nanocapsules: a platform for simultaneous cancer-targeted imaging and magnetically guided drug delivery, Chem. Eur. J., 18:12512-12521.

[17] Hamoudeh, M., Fessi, H. 2006. Preparation, characterization and surface study of poly-epsilon caprolactone magnetic microparticles, *Journal of Colloid and Interface Science,* 300(2), 584-590.

[18] Hoare, T., Santamaria, J., Goya, G.F., Irusta S., Lin D., Lau S., Padera R., Langer, R., Kohane D.S. 2009. A Magnetically Triggered Composite Membrane for On-Demand Drug Delivery, *Nanoletters,* 9(10), 3651-3657.

[19] Chomoucka, J., Drbohlavova, J., Huska, D., Adam, V., Kizek, R., Hubalek, J. 2010. Magnetic nanoparticles and targeted drug delivering, *Pharmacological Research,* 62, 144-149.

[20] Misak, H.E., Asmatulu, R., Gopu, J.S., Man, K.P., Zacharias, N.M., Wooley, P., Yang, S.Y. 2014. Albumin based nanocomposite sphere for advanced drug delivery system, *Biotechnol J*., 9, 163-170.

[21] Plassat, V., Wilhelm, C., Marsaud, V., Ménager, C., Gazeau, F., Renoir, J.M., Lesieur, S. 2011. Anti-estrogen-loaded superparamagnetic liposomes for intracellular magnetic targeting and treatment of breast cancer tumors, *Adv. Funct. Mater.,* 21, 83-92.

[22] Zhang F, Braun GB, Pallaoro A, Zhang Y, Shi Y, Cui D, Moskovits M, Zhao D, Stucky GD 2011. Mesoporous multifunctional upconversion luminescent and magnetic "nanorattle" materials for targeted chemotherapy, Nano Lett., 12:61-67.

[23] Widder, K.J., Morris, R.M., Poore, G.A., Howard, D.P., Senyei, A. E. 1983 Selective targeting of magnetic albumin microspheres containing low-dose doxorubicin-total remission in Yoshida sarcoma-bearing rats, *Eur. J. Cancer Clin. Oncol*., 19, 135-139.

[24] Pulfer, S.K., Ciccotto, S.L., Gallo, J.M. 1999. Distribution of small magnetic particles in brain tumor-bearing rats, *J. Neuro-Oncol*., 41, 99-105.

[25] Goodwin, S.C., Bittner, C.A., Peterson, C.L., Wong, G. 2001. Single-dose toxicity study of hepatic intra-arterial infusion of doxorubicin coupled to a novel magnetically targeted drug carrier, *Toxicol. Sci.*, 60, 177-83.

[26] Jia, Y., Yuan, M., Yuan, H., Huang, X., Sui, X., Cui, X., Tang, F., Peng, J., Chen, J., Lu, S., Xu, W., Zhang, L., Guo, Q. 2012. Co-encapsulation of magnetic Fe3O4 nanoparticles and doxorubicin into biodegradable PLGA nanocarriers for intratumoral drug delivery, *International Journal of Nanomedicine*, 7, 1697–1708.

[27] Jain, T.K., Richey, J., Strand, M., Leslie-Pelecky, D.L., Chris, A., Flask, C.A., Labhasetwar, V., 2008. Magnetic nanoparticles with dual functional properties: Drug delivery and magnetic resonance imaging, *Biomaterials*, 29, 4012-4021.

[28] Thomas, C.R., Ferris, D.P., Lee, J.H., Choi, E., Cho, M.H., Kim, E.S., Stoddart, J.F., Shin, J.S., Cheon, J., Zink, J.I. 2010. Noninvasive remote-controlled release of drug molecules in vitro using magnetic actuation of mechanized nanoparticles, *J. Am. Chem. Soc*., 132, 10623-10625.

[29] Hu, S.H., Chen, S.Y., Gao, X. 2012. Multifunctional nanocapsules for simultaneous encapsulation of hydrophilic and hydrophobic compounds and on-demand release. *ACS Nano*, 6, 2558-2565.

[30] Gun, S., Edirisinghe, M., Stride, E., 2013. Encapsulation of superparamagnetic iron oxide nanoparticles in poly-(lactide-co-glycolic acid) microspheres for biomedical applications, *Materials Science and Engineering C.*, 33, 3129-3137.

[31] Astete, C.E., Kumar, C.S.S.R, Sabliova, C.M., 2007. Size control of poly(d,l-lactide-co-glycolide) and poly(d,l-lactide-co-glycolide)-magnetite nanoparticles synthesized by emulsion evaporation technique, *Colloids and Surfaces A: Physicochem. Eng. Aspects,* 299, 209-216.

[32] Liu, X., Kaminski, M.D., Chen, H., Torno, M., Taylor, L.T., Rosengart, A.J., 2007. Synthesis and characterization of highly-magnetic biodegradable poly(D,L-lactide-co-glycolide) nanospheres, *Journal of Controlled Release*, 119, 52-58.

[33] Koneracka, M., Muckova, M., Zavisova, V., Tomasovicova, N., Kopcansky, P., Timko, M., Jurıkova, A., Csach, K., Kavecansky, V., Lancz, G., 2008. Encapsulation of anticancer drug and magnetic particles in biodegradable polymer nanospheres, *J. Phys.: Condens. Matter,* 20, 204151-156.

[34] Koppolu, B.P., Rahimi, M, Nattama, SP, Wadajkar, A, Nguyen, K. 2010. Development of multiple-layer polymeric particles for targeted and controlled drug delivery, *Nanomedicine: Nanotechnology, Biology, and Medicine* 6, 355-361.

[35] Zhao H, Saatchi, K., Hafeli, U.O., 2009. Preparation of biodegradable magnetic microspheres with poly(lactic acid)-coated magnetite, *Journal of Magnetism and Magnetic Materials*, 321, 1356-1363.

[36] Kini, S., Bahadur, D., Panda, D., 2011. Magnetic PLGA Nanospheres: A Dual Therapy for Cancer, *Ieee Transactions On Magnetics*, 47(10), 2882-2886.

[37] Shubhra, Q.T.H., Feczkó, T., Kardos, A.F., Tóth, J., Mackova, H., Horak, D., Dósa, G., Gyenis, J., 2014. Co-encapsulation of human serum albumin and superparamagnetic

iron oxide in PLGA nanoparticles: Part II. Effect of process variables on protein model drug encapsulation efficiency, *Journal of Microencapsulation*, 31:2, 156-165.

[38] Pérez, A., Mijangos, C., Hernández, R. 2014. Preparation of Hybrid Fe3O4/Poly(lactic-co-glycolic acid) (PLGA) Particles by Emulsion and Evaporation Method. Optimization of the Experimental Parameters, *Macromol. Symp*., 335, 62-69.

[39] Furlan, M., Kluge, J., Mazzotti, M., Lattuada, M., 2010. Preparation of biocompatible magnetite–PLGA composite nanoparticles using supercritical fluid extraction of emulsions, *J. of Supercritical Fluids*, 54, 348-356.

[40] Cai, K., Luo- Z., Hu- Y., Chen- X., Liao- Y., Yang- L., Deng- L., 2009. Magnetically triggered reversible controlled drug delivery from microfabricated polymeric multireservoir devices, *Adv. Mater*., 21, 4045-4049.

[41] Tudorachi, N., Chiriac, A.P., Mustata, F., 2015. New nanocomposite based on poly(lactic-co-glycolic acid) copolymer and magnetite. *Synthesis and characterization Composites: Part B*, 72, 150-159.

[42] Campardelli, R., Oleandro, E., Adami, R., Reverchon, E. 2014. Polymethylmethacrylate (PMMA) sub-microparticles produced by Supercritical Assisted Injection in a Liquid Antisolvent. *J. of Supercritical Fluids*, 92, 93-99.

[43] Espirito Santo, I., Campardelli, R., Albuquerque, E.C., de Melo, S.V., Reverchon, E. Della Porta, G., 2015. Liposomes Size Engineering by Combination of Ethanol Injection and Supercritical Processing, *Journal of Pharmaceutical Sciences*, 104 (11), 3842-3850.

[44] Della Porta, G., Falco, N., Reverchon, E. 2010. NSAID drugs release from injectable microspheres produced by supercritical fluid emulsion extraction, *Journal of Pharmaceutical Sciences*, 99, 1484-1499.

[45] Baldino, L., Cardea, S., De Marco, I., Reverchon, E. 2014. Chitosan scaffolds formation by a supercritical freeze extraction process, *J. of Supercritical Fluids*, 90, 27-34.

[46] Falco, N., Reverchon, E., Della Porta, G. 2013. Injectable PLGA/hydrocortisone formulation produced by continuous supercritical emulsion extraction. *International Journal of Pharmaceutics* 441, 589-597.

[47] Della Porta, G., Campardelli, R., Cricchio, V., Oliva, F., Maffulli, N., Reverchon, E. 2016. Injectable PLGA/Hydroxyapatite/Chitosan Microcapsules Produced by Supercritical Emulsion Extraction Technology: An In Vitro Study on Teriparatide/Gentamicin Controlled Release, *Journal of Pharmaceutical Sciences*, 105, 2164-2172.

[48] Cao, B., Tang, Q., Cheng, G. 2014. Recent advances of zwitterionic carboxybetaine materials and their derivatives. *Journal of Biomaterials Science, Polymer Edition*, 25 (14-15),1502-1513.

[49] Godzisz D., Ilczyszyn, M.M., Ilczyszyn, M. 2002. Classification and nature of hydrogen bonds to betaine. X-ray, 13C CP MAS and IR description of low barrier hydrogen bonds, *Journal of Molecular Structure*, 53 606 (1-3), 123-137.

[50] Hamoudeh, M., Al Faraj, A., Canet-Soulas, E., Bessueille, F., Leonard, D., Fessi, H. 2007. Elaboration of PLLA-based superparamagnetic nanoparticles: characterization, magnetic behaviour study and in vitro relaxivity evaluation, *International Journal of Pharmaceutics*, 338, 248-257.

[51] Wei Lai, C., Wang, Y.H., Lai, C.H., Yang, M.J., Chen, C.Y., Chou, P.T., Chan, C.S., Chi, Y., Chen, Y.C., Hsiao, J.H. 2008. Iridium-Complex-Functionalized Fe3O4/SiO2 Core/Shell Nanoparticles: A Facile Three-in-One System in Magnetic Resonance

Imaging, Luminescence Imaging, and Photodynamic Therapy, *Bio-nanomaterials*, 4(2), 218-224.

[52] Meikle, S.T., Piñeiro, Y., Bañobre López, M., Rivas, J., Santin, M. 2016. Surface functionalization superparamagnetic nanoparticles conjugated with thermoresponsive poly(epsilon-lysine) dendrons tethered with carboxybetaine for the mild hyperthermia-controlled delivery of VEGF, *Acta Biomaterialia*, 10.1016/j.actbio.2016.04.043.

[53] Gupta, A.K., Gupta, M. 2005. Synthesis and surface engineering of iron oxide nanoparticles for biomedical applications, *Biomaterials,* 26(18), 3995-4021.

[54] Powers, K.W., Brown, S.C., Krishna, V.B., Wasdo, S.C., Moudgil, B.M., Roberts, S.M. 2006. Research Strategies for Safety Evaluation of Nanomaterials. Part VI. Characterization of Nanoscale Particles for Toxicological Evaluation, *Toxicological Sciences*, 90(2), 296-303.

[55] Savolainena, K., Aleniusa, H., Norppaa, H., Pylkkänena, L., Tuomia, T., Kasperb, G. 2010. Risk assessment of engineered nanomaterials and nanotechnologies. A review, *Toxicology*, 269, 92-104.

FIGURE CAPTIONS

Figure 1. Field Emission-Scanning Electron Microscope (FE-SEM) images of PLGA and PLA microcarriers loaded with different MAG amounts. The microcarriers consistently showed spherical morphologies and mean sizes between 995-983 nm for PLGA and 837-853 nm for PLA. FE-SEM images of the empty devices are also reported for the purpose of comparison.

Figure 2. Emission Differential X-ray-Scanning Electron Microscope (EDX-SEM) image of PLGA microcarriers loaded with MAG at concentrations of 2.5 mg/g; single element maps related to iron (red), oxygen (light blue) and carbonium (green) are also shown. MAG nanoparticles showed uniform dispersion within the biopolymer devices (see red signals on SEM image) coupled with good encapsulation efficiency, as indicated from the iron concentration percentage calculated by the instrument.

Figure 3. TGA and FT-IR traces of PLGA/MAG and PLA/MAG and f-chitosan (*f-chi*) coated capsules. The thermal behavior was used to calculate the iron oxide loading after samples were heated to 750°C for the different formulations. Encapsulation Efficiency was 99% for all PLGA and 90% for PLA samples. FT-IR traces of different formulations consistently revealed the characteristic absorption peak for Fe_3O_4 at 580 cm^{-1} and those for poly-esters at about 1750 cm^{-1} (carbonyl groups), 1080 cm^{-1} (C–O–C stretching bands) and 1450 cm^{-1} (C–H stretching in methyl groups). The f-chitosan covering provided carboxybetaine moieties on the material with the slightly increase of methyl peak at 2937 cm^{-1}.

Figure 4. Zeta-Potential values of PLGA and PLA microcarriers suspension loaded with MAG at different pH; pure F_3O_3 nanoparticles suspensions, empty and *f*-chitosan coated carrier suspensions are also reported for comparison.

Figure 5. Field Emission-Scanning Electron Microscope (FE-SEM) images of PLGA and PLA carriers loaded with MAG and coated with *f*-Chitosan; the coated carrier preserved the spherical shape **(upper side)**. Histograms representing the Particle Size Distribution of coated and uncoated PLGA and PLA microcapsules also loaded with MAG (5 mg/g for PLGA; 4 mg/g for PLA): the coated particles showed a mean size increase of 0.2 μm **(lower left side)**. Transmission Electron microscope (TEM) image of the PLGA microcarrier, with the evidence of MAG loaded within (white spots) and the *f*-Chitosan coating that generate slightly irregular surface **(lower right side)**.

Figure 6. Release profiles from PLGA and *f-Chi*/PLGA microspheres loaded with fluorescein in PBS medium at 37°C **(left side)**; triggered release from PLGA/MAG, *f-Chi*/PLGA/MAG and PLA/MAG microcapsules all loaded with the same amount of Fluorescein (8 mg/g) and with the same content of MAG (4 mg/g) in PBS medium at 37°C by Alternating Magnetic Field (AMF) **(right side).**

Table 1. List of microcapsules produced by SEE, mean size (MS) and standard deviation (±), drug encapsulation efficiency expressed as percentage (EE%) and drug real loadings expressed as mg/g (g is referred to the amount of biopolymer contained in the product); Z-Potential (Zp) values measured at pH 5.5. MAG: iron oxide nanoparticles; Fluo: fluorescein; *f*-Chi: functionalized chitosan.

Microcapsule composition	**MS (nm)**	**Mag (EE%)**	**Mag (mg/g)**	**Fluo (EE%)**	**Fluo (mg/g)**	**Zp pH 5.5 (mV)**
PLGA/MAG	880 (±104)	99	1.2	--	--	-3.01
PLGA/MAG	995 (±126)	99	2.5	--	--	-5.6
PLGA/MAG	971 (± 118)	99	5	--	--	-4.2
PLGA/MAG/Fluo	983 (±148)	99	5	78	7.8	-5.5
PLA/MAG	837(±119)	90	1	--	--	-4.1
PLA/MAG	828 (±124)	90	2	--	--	-2.1
PLA/MAG	853 (± 108)	90	4	--	--	-2.6
f-chi-PLGA/MAG	1103 (± 110)	99	5		--	31.7
f-chi-PLGA/MAG/Fluo	1114 (± 130)	99	5	80	8.0	34.5
f-chi-PLA/MAG	1098 (± 118)	99	5	--	--	27.7

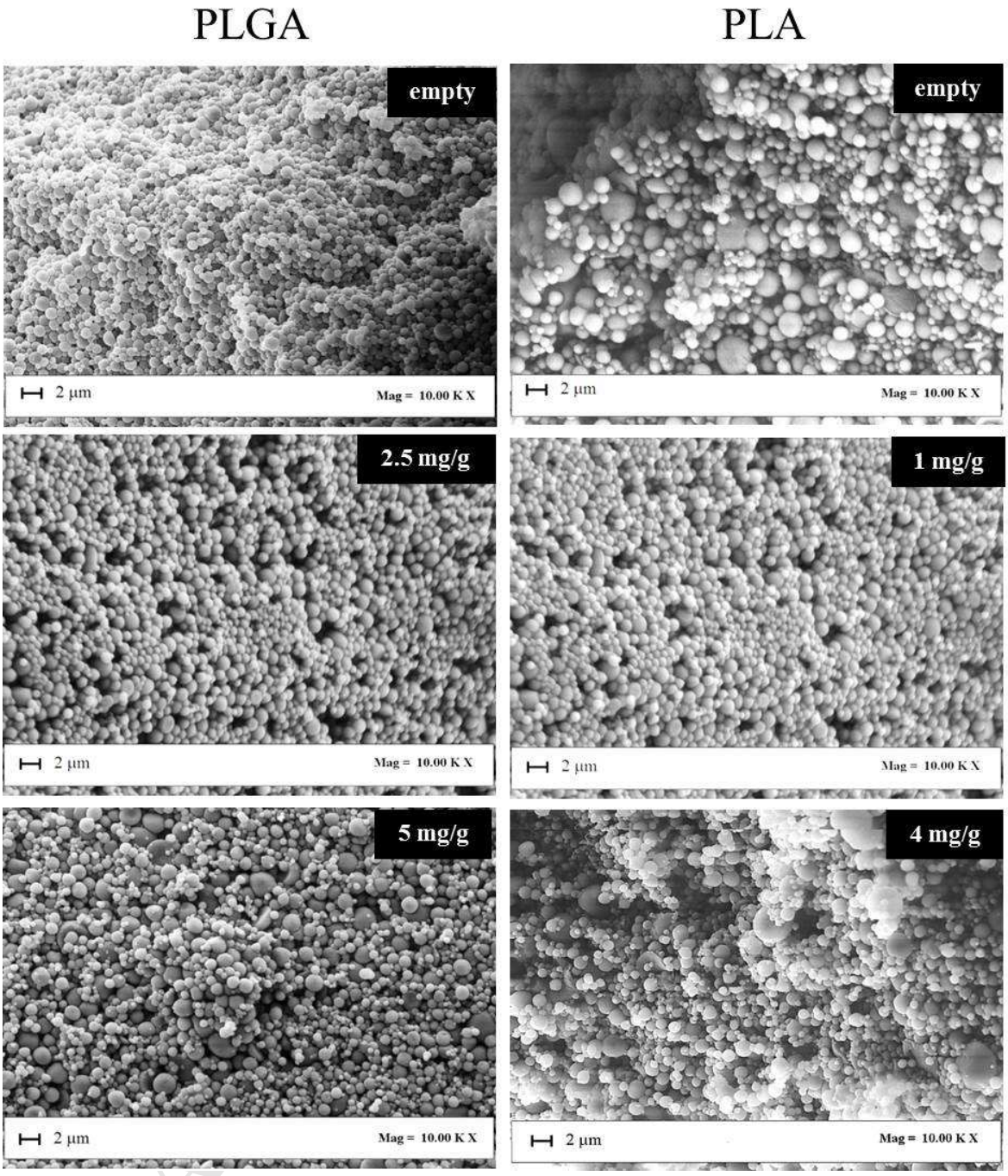
PLGA
PLA
empty
empty
2 µm
Mag = 10.00 K X
2 µm
Mag = 10.00 K X
2.5 mg/g
1 mg/g
2 µm
Mag = 10.00 K X
2 µm
Mag = 10.00 K X
5 mg/g
4 mg/g
2 µm
Mag = 10.00 K X
2 µm
Mag = 10.00 K X

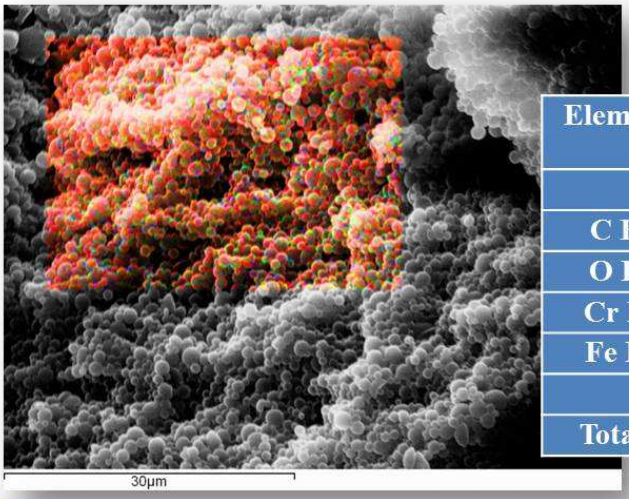

Element	App	Intensity	Weight %
	Conc.	Corrn.	
C K	41.25	1.2224	56.98
O K	11.27	0.5135	37.04
Cr K	2.64	0.8001	5.57
Fe K	0.18	0.7811	0.40
Totals			100.00

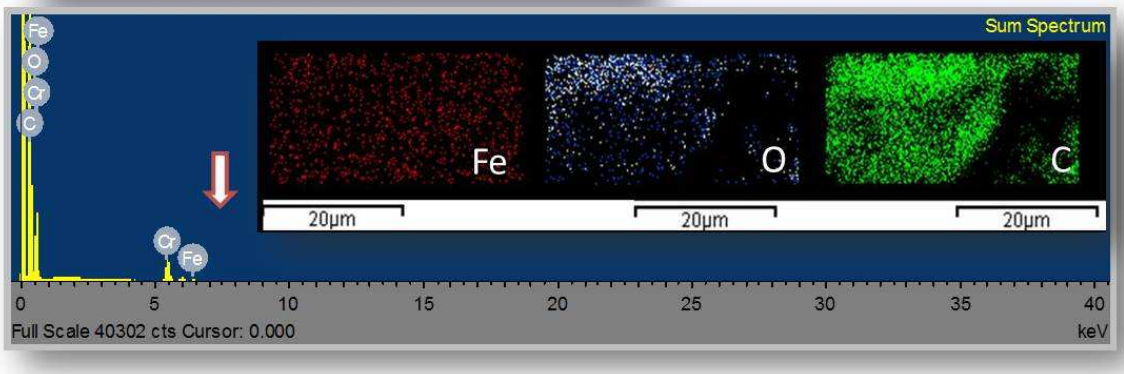

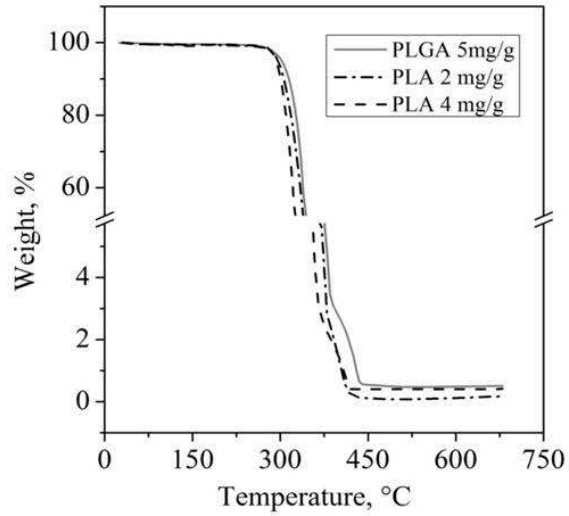
PLGA 5mg/g
PLA 2 mg/g
PLA 4 mg/g
Weight, %
Temperature, °C

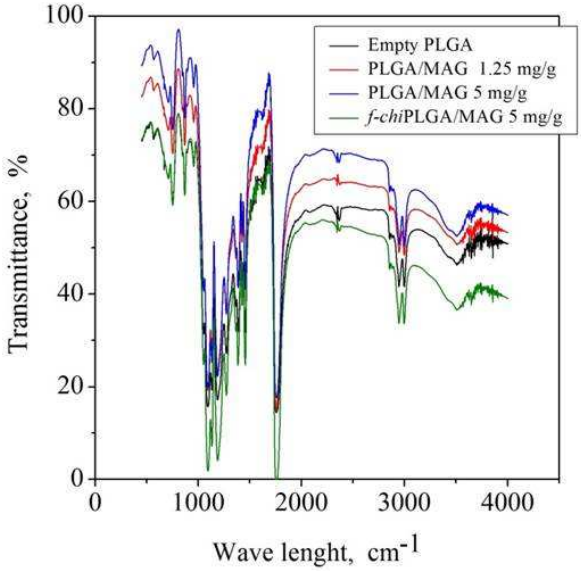
Empty PLGA
PLGA/MAG 1.25 mg/g
PLGA/MAG 5 mg/g
f-chiPLGA/MAG 5 mg/g
Transmittance, %
Wave lenght, cm-1

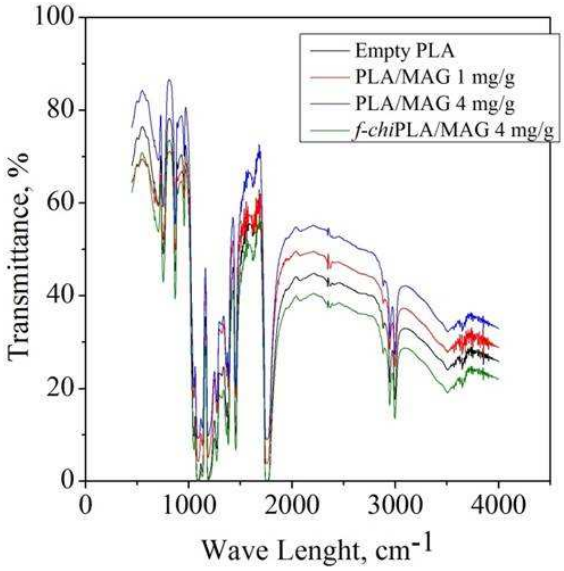
Empty PLA
PLA/MAG 1 mg/g
PLA/MAG 4 mg/g
f-chiPLA/MAG 4 mg/g
Transmittance, %
Wave Lenght, cm-1